Research Article Vol. 6, No. 3 / March 2019 / Optica 274

Rapid broadband characterization of scattering medium using hyperspectral imaging

Antoine Boniface,[1,†] Ivan Gusachenko,[2,*,†] Kishan Dholakia,[2] and Sylvain Gigan[1]

[1]Laboratoire Kastler Brossel, Sorbonne Université, École Normale Supérieure–Paris Sciences et Lettres (PSL) Research University, CNRS, Collège de France, 24 rue Lhomond, 75005 Paris, France
[2]SUPA, School of Physics & Astronomy, University of St Andrews, North Haugh, St Andrews KY16 9SS, UK
*Corresponding author: ivan.gusachenko@gmail.com

Received 19 September 2018; revised 7 December 2018; accepted 7 December 2018 (Doc. ID 346381); published 4 March 2019

Scattering of a coherent ultrashort pulse of light by a disordered medium results in a complex spatiotemporal speckle pattern. The form of the pattern can be described by knowledge of a spectrally dependent transmission matrix, which can in turn be used to shape the propagation of the pulse through the medium. We introduce a method for rapid measurement of this matrix for the entire spectrum of the pulse based on a hyperspectral imaging system that is close to 2 orders of magnitude faster than any approach previously reported. We demonstrate narrowband as well as spatiotemporal refocusing of a femtosecond pulse temporally stretched to several picoseconds after propagation through a multiply scattering medium. This enables new routes for multiphoton imaging and manipulation through complex media.

https://doi.org/10.1364/OPTICA.6.000274

1. INTRODUCTION

Light propagation in a disordered medium gives rise to scattering. When the size of the medium becomes large compared to the scattering mean free path, the transmitted light is multiply scattered. This poses a major depth limitation for conventional imaging techniques, in particular imaging through biological tissues, due to exponential attenuation of unscattered light. It is also a significant limitation to other light–matter interaction applications such as optical manipulation. Nonetheless, owing to the linearity and coherence of elastic scattering, the scattered light retains its coherence. However, due to the complexity of the scattering process, a coherent narrowband continuous wave laser typically gives rise to an output interference pattern in the form of speckle. The scattering process can then be described by means of the transmission matrix (TM) of the medium, linking the input field to the output field. The measurement of the transmission matrix and the ability to control the incident wavefront by means of dynamic diffractive optics have opened the possibility to control speckle patterns and shape the output in complex media. It has created a wealth of new applications, in particular in scattering tissue imaging and in mesoscopic physics that studies such elusive phenomena as the presence of open and closed channels in scattering media [1].

An even more challenging issue is the measurement and control of the temporal or spectral degrees of freedom of broadband light after multiple scattering. This happens when a short pulse is temporally dispersed due to the large distribution of path lengths in the medium, which in the diffusive regime scales as L^2/l^* where L is the medium thickness and l^* the transport mean free path. Tackling this issue would open prospects for performing nonlinear and multiphoton imaging through tissue, for example [2,3]. In particular, by determining a multispectral TM (MSTM) of a medium (i.e., measuring multiple monochromatic TMs over a large spectral band), one can achieve full control of a transmitted ultrashort pulse both in time and space, achieving narrowband or ultrashort focusing of light, for instance [4]. Although this method has proven its efficiency, its technical complexity precludes its broad use. Primarily, it requires a pulsed laser that is also capable of tunable CW operation. To determine the matrix, a sequential acquisition procedure is required. Each monochromatic TM takes a few minutes to measure depending on the number of input pixels and the speed of the optical element used to generate input modes [typically a spatial light modulator (SLM)]. The number of TMs to be measured scales linearly with the spectral bandwidth to be measured and inversely with the spectral resolution required. The former is linked to the laser pulse duration and the latter to the medium dwell time. For highly dispersive media (a large number of independent wavelengths) and for a large input pixel count, the measurement time can be several hours, thus limiting the approach to proof of principle demonstrations in static media.

Here, we implement a form of a hyperspectral imaging technique to parallelize the full MSTM measurement of a highly dispersive complex medium. A microlens array and a diffraction grating are used to encode both spatial and spectral information of

the output speckle on a single camera. The acquisition time becomes independent of the pulse lengthening and does not require a tunable source. We demonstrate the power of this approach for focusing and pulse control, and report on the advantages of the technique for a highly dispersive medium, in a regime where the above, more conventional method would be impractical because of unrealistic measurement time. Here, we demonstrate a speedup of up to 2 orders of magnitude in the MSTM measurement time.

2. METHODS

A. MSTM Acquisition

The TM of a complex medium links the input modes to the output modes in a linear manner. In our case, the input modes were Hadamard patterns on the SLM, and the output modes were camera pixels. To measure a monochromatic TM, in short, one first illuminates an SLM with a CW laser, and then projects a set of input patterns on the SLM that form a complete basis of orthogonal modes, recording the resulting speckle patterns on the camera. Using either off-axis [5,6] or phase-stepping holography [7], one can thus deduce the TM. These conditions were subsequently relaxed, for instance allowing determination of the TM solely from intensity measurements without interferometry or with random binary input patterns [8].

A scattering medium has a spectrally dependent response characterized by a spectral correlation bandwidth $\delta\lambda_m$, which is inversely proportional to the average confinement time of light in the medium [9,10]. Specifically, $\delta\lambda_m$ designates a wavelength shift upon which the correlation function between the two monochromatic speckle patterns drops to 0.5 [11]. Consequently, an ultrashort pulse with bandwidth $\Delta\lambda^{\text{laser}} > \delta\lambda_m$ is both spectrally and temporally distorted after its propagation through a scattering medium. Quantitatively, $N_\lambda = \frac{\Delta\lambda^{\text{laser}}}{\delta\lambda_m}$ describes the number of spectral degrees of freedom [12]. This ratio determines the spectral sampling of the MSTM acquisition required to fully describe the scattered pulse both spectrally and temporally.

The MSTM acquisition procedure builds upon an approach described in our previous work [13]. We divide the SLM in $N_{\text{SLM}} = 64 \times 64 = 4096$ macropixels and generate a full Hadamard basis on this grid as the input probe modes. The MSTM elements are obtained by phase-step interferometry of the probe mode with the reference arm (see Fig. 2). As the reference and signal arms do not share a common path, random phase drifts and fluctuations between them due to temperature gradients and airflow have to be considered. To account for this, the phase drift was monitored and corrected for as shown earlier [14]. Once measured, the MSTM proved to be stable, as we were typically able to perform focusing with it the next day after acquisition.

The crucial difference for our approach versus the conventional method [9,12] for MSTM acquisition consists in using broadband pulses for illumination and a hyperspectral imaging arm for detection. This allows us to acquire matrix elements for all the constituent wavelengths of the pulse simultaneously.

B. Principle and Limitations of Hyperspectral Imaging with a Microlens Array

Snapshot hyperspectral imaging (HSI) comes in different forms [15] and exploits various strategies for coupling spatial and spectral degrees of freedom using custom arrays of optical

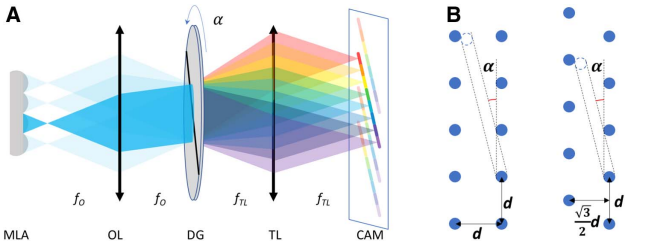

Fig. 1. Design of the "snapshot" hyperspectral imaging approach. (A) Diagram of the optical setup. MLA, microlens array; OL, objective lens; DG, diffraction grating; TL, tube lens; CAM, camera. (B) Spectra packing for (left) square and (right) hexagonal array.

elements (filters [16], prisms [17], mirrors [18]) or even scattering media [19].

In our work, to simultaneously acquire both spatial and spectral data (3D data) on a single 2D imaging array, we implement a so-called integral field spectroscopy with a microlens (lenslet) array [15]. The general procedure was first proposed by Courtès [20] for astronomy and gained renewed interest in 2006 [21] with a design of a compact snapshot hyperspectral camera. However, this elegant technique has far broader implications than has been recognized, such as the one described in our study.

The schematics of the optical design is shown in Fig. 1(A). A microlens array (MLA) samples the incoming field and creates an array of focused spots. The spots are then collimated by the objective lens (OL) into beamlets that are incident on a diffraction grating (DG). The tube lens (TL) images the spectrally dispersed array of spots onto the camera (CAM). Crucially, the microlens array is slightly rotated with respect to the dispersion axis of the grating to enable dense packing of the line spectra on the camera without overlap [see Fig. 1(B)]. In this configuration, all the spectral components of each spatial pixel (individual microlens) are simultaneously captured within one frame, allowing for the degree of parallelization equal to the number of spectrally resolvable spots.

To determine the number of resolvable spots in the spectrum, consider Fig. 1(B). For the microlens array pitch d, and the diameter of the spot it creates at the focus, s, one can find an angle α

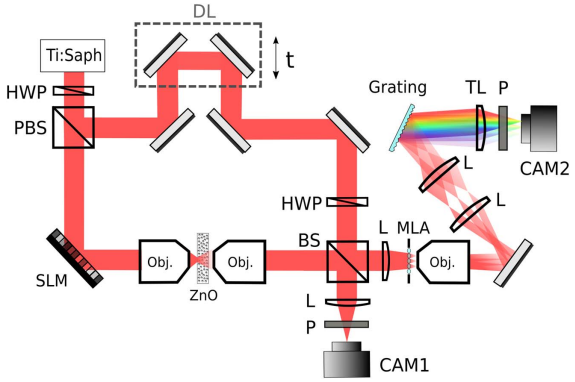

Fig. 2. Experimental setup. A femtosecond Ti:Sapphire laser is expanded onto a phase-only spatial light modulator (SLM). The scattering medium is a thick (~100 μm) sample of ZnO particles, placed in between two microscope objectives. A delay line (DL) adjusts delay between reference beam and scattered light. The two beams recombine on the beam splitter (BS) and are imaged on CCD2 or onto the microlens array (MLA). Lens (L), half-wave plate (HPW), polarizer (P), polarized beam splitter (PBS), microscope objective (Obj.), tube lens (TL).

between an array lattice vector and the dispersion axis such that the spectra from adjacent spots do not overlap. As can be determined from the figure, the minimum angle that satisfies this requirement is $\alpha = 2\arcsin(s/2d) \approx s/d$. The number of resolvable spots is then $N_{\lambda\square} \sim d/\sin(\alpha) \cdot 1/s = (d/s)^2$ for a square lattice and $N_{\lambda\Delta} \sim \frac{\sqrt{3}}{2}(d/s)^2$ for a hexagonal one. For low-NA microlens arrays, the aberrations are negligible and the resolvable spot size s is the radius of an Airy disk $s = r_{\text{Airy}} = 0.61\lambda/\text{NA}$.

To estimate the maximum bandwidth $\Delta\lambda$ we may achieve without overlap, consider the length of the spectrum track on the camera. On one hand, it amounts to $\Delta\lambda \frac{d\beta}{d\lambda} f_{\text{TL}}$, where $\frac{d\beta}{d\lambda}$ is the dispersion of the grating. On the other hand, it should be smaller than d^2/s (square lattice) magnified by $f_{\text{TL}}/f_{\text{OL}}$. Therefore, $\Delta\lambda < \frac{d^2}{s f_{\text{OL}}}(\frac{d\beta}{d\lambda})^{-1}$, and the spectral resolution is $\delta\lambda_{\text{HSI}} = \Delta\lambda/N_\lambda$.

Finally, the number of spatial pixels (i.e., distinct spectra from different microlenses) that fit on the detector of the size D depends on the magnification from the MLA focus to the camera and can be estimated as $N_{xy} \sim (D/d \cdot f_{\text{OL}}/f_{\text{TL}})^2$. The expressions for N_{xy}, N_λ, and $\Delta\lambda$ allow one to easily optimize them for a given application.

C. Experimental Setup

Figure 2 shows the experimental setup to measure the multispectral transmission matrix and characterize its ability to focus a pulse of light at the output of a dispersive (thick) scattering medium, spatially, spectrally, and temporally. A Ti:Sapphire laser source (MaiTai, Spectra Physics) produces a 120 fs ultrashort pulse, centered at 800 nm with a spectral bandwidth of 13.8 nm FWHM. The beam is split in two different beams: reference path and a sample path. In the sample path, a phase-only SLM (LCOS-SLM, Large 512 × 512, Meadowlark) subdivided in 64 × 64 macropixels is conjugated with the back focal plane of a microscope objective (Olympus Plan N, 20×, NA 0.40), which illuminates a scattering medium made of ZnO nanoparticles (thickness ≃100 μm). The transmitted speckle is collected with another microscope objective (Olympus LMPlan FI, 100×, NA 0.85). The output beam is recombined with the reference on a beam splitter (BS), and the hologram can either be sent into the hyperspectral arm detailed in Subsection 2.B or recorded on a CCD camera (CAM1, Allied Vision, Manta G-046). CAM1 is then effectively used to independently validate the performance of the HSI focusing.

D. Hyperspectral Imaging Calibration

For our experiment we use a hexagonal microlens array with 30 μm pitch and NA of 0.16 (SUSS Microoptics, 18-00079), objective lens of $f_{\text{OL}} = 12$ mm (an Olympus 20 × 0.4NA∞ objective followed by a 1.33× telescope), Thorlabs GR25-0608 grating with $\frac{d\beta}{d\lambda} = 0.62$ mrad/nm, tube lens of $f_{\text{TL}} = 50$ mm, and Basler acA1300-30um CCD camera (CAM2). Those parameters yield $N_{\lambda\Delta\,\max} \simeq 72$, $\delta\lambda_{\text{HSI}} \simeq 0.40$ nm, and $\Delta\lambda_{\max} \simeq 29$ nm. As the required bandwidth to accommodate the laser spectrum was somewhat much narrower than 29 nm (13.8 nm FWHM, 23 nm at >15% level), we traded some bandwidth by tilting the microlens array more to reduce coupling between neighboring spectra. This yielded $\Delta\lambda \simeq 23$ nm and $N_{\lambda\Delta} \simeq 57$. In accordance, we set the number of spectral bins at 90 to moderately oversample the spectra.

The number of hexagonal spatial pixels captured by CAM2 was 198, which is roughly equivalent to a 15 × 13 rectangular grid area. It is noteworthy that the wavelength range can be tailored to an application, and pulses with bandwidth as broad as, e.g., 100 nm can also be shaped with nanometer resolution.

To calibrate the HSI setup, we performed a wavelength scan with the laser in CW mode to acquire spot patterns at different wavelengths. The patterns were processed by a custom Matlab script to yield a conversion matrix between pixels of the camera and spatiospectral pixels of the resulting hyperspectral image. This matrix was used to convert raw images from CAM2 into arrays of spectra. Additional information on the calibration can be found in Supplement 1.

3. RESULTS

In the following section we report on performances of the technique through a different wavefront shaping experiment, showcasing the ability of the measured MSTM to allow spatial and temporal focusing of a pulse.

A. Spectral Control

Knowledge of the MSTM for all the N_λ independent spectral components provides the means to control the light transmission spatially and spectrally with an SLM. As shown previously, this can be used to focus a single spectral component of a broadband pulse at a given spatial position [9,12]. The required input field is calculated by first choosing the monochromatic TM for the desired wavelength and then performing complex conjugation on the TM column corresponding to the desired spatial position [9]. For a phase-only SLM used in our study, the displayed mask is the phase of the input field.

Note that in our method that uses hyperspectral imaging, all possible spatiospectral combinations have a dedicated physical pixel on the detector. The spatiospectral focusing is thus conceptually a "conventional" digital conjugation focusing into such a pixel.

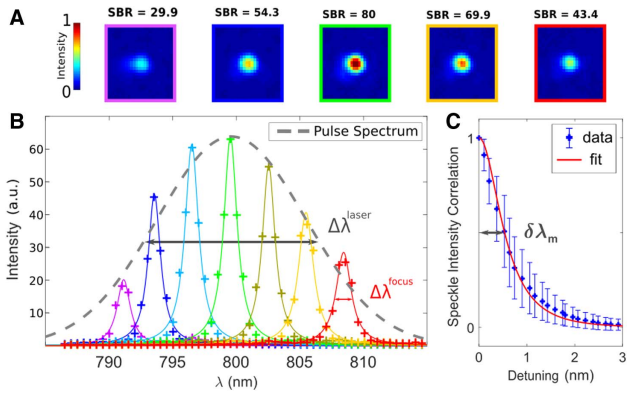

Fig. 3. Simultaneous spatiospectral focusing. (A) Spatial foci at different wavelengths measured on CCD1. (B) Spectral profiles of the corresponding foci (measured on CCD2–Lorentzian fit) ($\Delta\lambda^{\text{focus}} = 1.30 \pm 0.05$ nm). Pulse spectrum measured with a spectrometer (HR4000, OceanOptics) is superimposed ($\Delta\lambda^{\text{laser}} = 13.8$ nm). (C) Speckle correlation of the medium with $\delta\lambda_m \simeq 0.53$ nm, corresponding to $N_\lambda \simeq 26$.

Simultaneous spatiospectral focusing of the scattered light is shown in the Fig. 3. We digitally scan through several SLM masks corresponding to the same spatial but different spectral positions; the corresponding focal intensities are shown in Fig. 3(A). As for the spectral focusing we target only the corresponding wavelength of interest; other wavelengths contribute to the background. Therefore, the signal-to-background ratio (SBR) varies across the pulse spectrum and is generally proportional to the spectral intensity of the original pulse.

We emphasize that spectral profiles in Fig. 3(B) are reconstructed directly from the CAM2, since it operates as an integral field spectrometer. All the spectral foci have approximately a Lorentzian shape (that is, a Fourier transform of the exponentially decaying time of flight distribution [22]) characterized by the same FWHM $\Delta\lambda^{\text{focus}} = 1.30 \pm 0.05$ nm. The spectral width of the focus is closely related to the spectral correlation width $\delta\lambda_m$ of the medium [23]: $\Delta\lambda^{\text{focus}} \simeq 2\delta\lambda_m$. The latter is measured by correlating monochromatic speckle intensity images with respect to the wavelength scanning, as in Refs. [9,24].

When recording intensity, the SBR of the focus should be proportional to the number of spatial degrees of freedom exploited on the SLM [25]. When the laser is broadband, the SBR for monochromatic focusing should be $\text{SBR} = \frac{\pi}{4}\frac{N_{\text{SLM}}}{N_\lambda}$ [9], inversely proportional to N_λ [26]. For all the experiments presented in the article we choose to use $N_{\text{SLM}} = 64 \times 64$ SLM pixels, a good trade-off between the SBR and the measurement time. Here, we report an experimental enhancement $\simeq$80, about 2/3 of the theoretical maximum. This deviation is typical in wavefront shaping experiments and can be attributed essentially to measurement noise [27,28].

B. Temporal Shaping

To show that the MSTM measured with the HSI contains accurate information about the phase relationship between different spectral components, we performed broadband focusing and verified the ability of the MSTM to control temporally a pulse, by adjusting the relative phases and amplitudes of all the N_λ spectral components [12].

More precisely, the desired field E^{in} is obtained the following way:

$$E_j^{\text{in}} = \sum_{l=1}^{N_\lambda} a_l E_j^{\text{in}}(\lambda_l) e^{i\theta_l}, \tag{1}$$

where $E^{\text{in}}(\lambda_l)$ is a monochromatic input field required to focus the wavelength λ_l on the jth spatial coordinate.

As an example, temporal recompression of the pulse close to its Fourier-limited duration was performed by imposing a flat spectral phase ($\theta_l = \text{const}$, $\forall l \in [1; N_\lambda]$). Experimental results are presented in Fig. 4. Temporal envelopes are retrieved from the interference between the unknown stretched pulse and the external reference ultrashort pulse as a function of the delay t set by a delay line DL (see Fig. 2) via interferometric cross-correlation [29]. The decaying tail of the temporal profile was fitted with an exponential to extract the characteristic broadened pulse duration that characterizes the pulse stretching (see Supplement 1 Section 2). Importantly, the measurement was performed on the camera, ensuring that the measurement is independent from the spectrometer. When the flat spectral phase is applied, we observe a spatiotemporal focus at time t_0 when the MSTM was recorded. With the same matrix, the refocused pulse can be temporally delayed or advanced with respect to t_0 by adding a positive or negative spectral phase ramp, respectively [inset on Fig. 4(A)]. The temporal curves are averaged over 10 different spatial positions. For the three temporal profiles we estimate average FWHM of the refocused pulse convoluted with the reference is $\simeq$203 fs. This is consistent with the initial pulse duration (>120 fs) given it is convoluted with the reference pulse. Corresponding spatial foci recorded with CAM1 are shown with their respective SBR on Fig. 4(B).

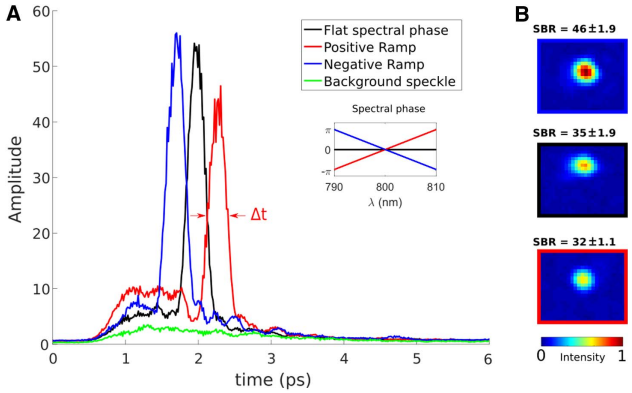

Fig. 4. Temporal focusing of the beam. (A) Temporal profiles of the amplitude of the speckle background and temporally refocused pulses for the medium with $N_\lambda = 25$. Profiles are averaged over 10 different spatial positions. Over the three temporal envelopes FWHM for the field amplitude is estimated to $\Delta t = 287 \pm 8$ fs. For the intensity, the corresponding pulse width is $\Delta t/\sqrt{2} \simeq 203$ fs (Gaussian shape). Inset: different spectral phase ramps' relations applied to the spectral components. Slope of the ramp determines the pulse arrival delay time with respect to the pulse with a flat spectral phase. (B) Images of corresponding spatial foci on CAM1. The SBR is intrinsically linked with the arrival time of the scattered pulse, in accordance with the arrival time intensity distribution.

As discussed in Ref. [12], the SBR scales inversely with N_λ and is maximum when the arrival time of the pulse coincides with the maximum of the time-of-flight distribution.

C. High Performance for Very Thick Media

A major advantage of our technique is speed. Unlike sequential measurements [12], the acquisition time does not depend on N_λ. More precisely, for a given N_λ, an HSI system can be designed so that all monochromatic TMs can be acquired in parallel. The spectral resolution for the MSTM is set by the microlens array and the grating, while its spatial size is determined by the total camera pixel counts.

It makes a significant difference for characterization of very thick media. We showcase this speed advantage by reproducing the experiment with an extremely dispersive medium [spectral bandwidth $\delta\lambda_m = 0.17$ nm, $N_\lambda = 80$, see Fig. 5(A)], which would be too long to characterize sequentially. For illustrative purposes we plot spectral profiles for only seven spectral components in Fig. 5(B). The Lorentzian fit of the curves gives a FWHM estimation $\Delta\lambda^{\text{focus}} = 0.62 \pm 0.02$ nm, while speckle correlations with respect to λ yield $2\delta\lambda_m \approx 0.35$ nm, therefore slightly exceeding the finite spectral resolution of the HSI, which is estimated at $\delta\lambda_{\text{HSI}} = 0.4$ nm. The resolution might have been further deteriorated by a finite angular spread of the input light, as will be discussed below.

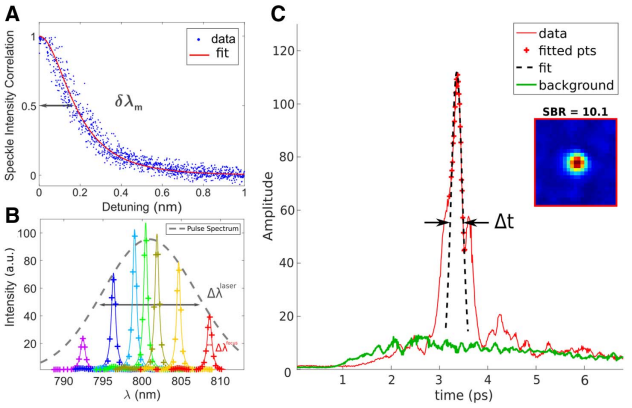

Fig. 5. Spatiotemporal focusing behind very thick media. (A) Intensity correlation curve that yields $\delta\lambda_m = 0.17$ nm. This corresponds to $N_\lambda = 80$ spectral degrees of freedom. (B) Spectral profile of simultaneous spatiospectral focusing (measured on CCD2–Lorentzian fit) ($\Delta\lambda^{\text{focus}} = 0.62 \pm 0.02$ nm). The pulse spectrum measured with a spectrometer is superimposed ($\Delta\lambda^{\text{laser}} = 13.8$ nm). (C) N_λ spectral components of the pulse are focused with a flat spectral phase to achieve temporal recompression of the pulse to $\Delta t = 270$ fs in amplitude (averaged over 10 different spatial positions). For the intensity, the corresponding pulse width is $\Delta t/\sqrt{2} \simeq 191$ fs (consistent with the incident pulse duration). Inset: best spatial focus.

The spatiotemporal recompression of the pulse produced by focusing all the $N_\lambda = 80$ spectral components with a flat spectral phase is shown on Fig. 5(C). The high number of spectral components reduces the SBR for a given number of SLM modes, preventing high-fidelity temporal shaping. Nevertheless, the central dominant peak of the temporal profile achieves close to initial duration (≃191 fs, for the corresponding intensity profile).

4. DISCUSSION

In our work we have demonstrated the potential for parallelizing an MSTM acquisition with a snapshot hyperspectral imaging system. While pushing the limits of the method in terms of throughput was outside the present scope, such multispectral acquisition can be made extremely fast. The microlens array used in this study has >5000 elements, limiting the number of resolvable spatial pixels. Given a ∼80 spectral bin resolution this array provides at $\lambda = 800$ nm; a 4 Mpix camera is sufficient to resolve each spatiospectral bin ($4\ \text{Mpix}/(5000 \cdot 80) \simeq 10$ pixels $\approx 3 \times 3$). We envisage that the number of spatial pixels can be further improved. First, exploiting the memory effect in scattering media [30] would allow scanning of the focused spots over a small range (at least 3 × 3 grid) in their close vicinity, thus increasing the number of pixels by an order of magnitude. Second, while the lenslet array HSI we used is straightforward and intuitive, other snapshot hyperspectral methods exist that make 10-fold more efficient use of the camera pixels [18] at the cost of increased complexity.

CameraLink and CoaXPress interface cameras can steadily produce 180 fps at 4 Mp resolution, meaning that a full MSTM for 5000 spatial pixel ×80 spectral bins and 4096 input SLM modes can be acquired in 91 s. Fast SLMs available on the market (>500 Hz with LCoS SLM and >20 kHz with digital micromirror devices) easily satisfy the 180 fps speed requirement.

It is natural to extend this technique to other scattering media. In our case of a highly scattering layer with a huge number of spatial degrees of freedom, we naturally faced a tradeoff between the number of spatial modes we can record simultaneously and the number of spectral bins we can resolve. On the other hand, wavefront shaping in optical fibers with limited number of modes (∼1000) is of great interest for developing ultra-compact endoscopes with fluorescence [31–33], two-photon fluorescence [34], and Raman [35] contrasts. Here, all the spatial modes could be spectrally dispersed on a single detector, allowing for full spatiospectral characterization of a multimode fiber. The relatively small number of modes (i.e., required image size) allows the use of high-speed cameras with internal memory, for which the full MSTM can be acquired in ∼1 s (e.g., 3200 fps at 1 Mp with Photron MINI WX100). We therefore speculate that this method has great potential for multiphoton or multicolor endoscopy, where the calibration time is critical. We can hope that in combination with recent strategies for TM acquisition without access to the fiber distal end [36], our method would enable video-rate multiphoton microendoscopy with dynamic bending correction.

A notable limitation of the lenslet-based HSI is its sensitivity to the wavefront shape. Indeed, its optical design is very similar to a Shack–Hartmann wavefront sensor. To limit this effect, the angular spread of the probed light should be much smaller than the NA of the microlenses. This requirement is satisfied in our system ($\text{NA}_{\text{signal}} \approx 0.01 \ll 0.16$); however, it is possible that it slightly contributes to the degradation of the spectral resolution as seen in Fig. 5 for the very thick medium. This limitation is, however, not fundamental, as it suffices to magnify the probed beam and to use arrays with a bigger lenslet size and/or a higher NA.

Note that our method does not strictly require wavelength calibration, as the MSTM can be measured in arbitrary wavelength units, and the beam can be focused spatiospectrally or spatiotemporally all the same. On the contrary, for conventional MSTM acquisition the CW operation cannot be dispensed with, as all the monochromatic TMs must be acquired separately. At the same time, having such a CW mode is more an exception rather than a rule for turnkey femtosecond lasers. Our method thus heavily reduces the instrumental requirements for MSTM acquisition as it eliminates the need for the tunable CW regime. If desired, the absolute wavelength calibration can still be provided by an appropriate gas calibration source (e.g., Argon lamp near 800 nm).

In conclusion, we have implemented a method for rapid multispectral TM measurement that can speed up acquisition by nearly 2 orders of magnitude. Our technique can be applied to various scattering and dispersive media and holds great promise for both fundamental and applied studies of the light transport in complex media. Most important, modern systems for deep tissue imaging rely on multiphoton excitation and thus on ultrashort pulses to be delivered within scattering tissues. Hence, rapid tissue characterization enabled by our technique can be revolutionary for future multiphoton imaging *in vivo*.

Funding. Engineering and Physical Sciences Research Council (EPSRC) (EP/R004854/1); Scottish Universities Physics Alliance (SUPA) (SFC H17014); H2020 European Research Council (ERC) (SMARTIES–724473).

See Supplement 1 for supporting content.

†These authors contributed equally to this work.

REFERENCES

1. S. Rotter and S. Gigan, "Light fields in complex media: mesoscopic scattering meets wave control," Rev. Mod. Phys. **89**, 015005 (2017).
2. J. Aulbach, B. Gjonaj, P. M. Johnson, A. P. Mosk, and A. Lagendijk, "Control of light transmission through opaque scattering media in space and time," Phys. Rev. Lett. **106**, 103901 (2011).
3. O. Katz, E. Small, Y. Bromberg, and Y. Silberberg, "Focusing and compression of ultrashort pulses through scattering media," Nat. Photonics **5**, 372–377 (2011).
4. M. Mounaix, D. M. Ta, and S. Gigan, "Transmission matrix approaches for nonlinear fluorescence excitation through multiple scattering media," Opt. Lett. **43**, 2831–2834 (2018).
5. Y. Choi, T. D. Yang, C. Fang-Yen, P. Kang, K. J. Lee, R. R. Dasari, M. S. Feld, and W. Choi, "Overcoming the diffraction limit using multiple light scattering in a highly disordered medium," Phys. Rev. Lett. **107**, 023902 (2011).
6. D. Akbulut, T. Strudley, J. Bertolotti, E. P. Bakkers, A. Lagendijk, O. L. Muskens, W. L. Vos, and A. P. Mosk, "Optical transmission matrix as a probe of the photonic strength," Phys. Rev. A **94**, 043817 (2016).
7. S. Popoff, G. Lerosey, R. Carminati, M. Fink, A. Boccara, and S. Gigan, "Measuring the transmission matrix in optics: an approach to the study and control of light propagation in disordered media," Phys. Rev. Lett. **104**, 100601 (2010).
8. A. Drémeau, A. Liutkus, D. Martina, O. Katz, C. Schülke, F. Krzakala, S. Gigan, and L. Daudet, "Reference-less measurement of the transmission matrix of a highly scattering material using a DMD and phase retrieval techniques," Opt. Express **23**, 11898–11911 (2015).
9. D. Andreoli, G. Volpe, S. Popoff, O. Katz, S. Grésillon, and S. Gigan, "Deterministic control of broadband light through a multiply scattering medium via the multispectral transmission matrix," Sci. Rep. **5**, 10347 (2015).
10. J. Aulbach, A. Tourin, and A. Lagendijk, *Spatiotemporal Control of Light in Turbid Media* (Universiteit of Twente, 2013).
11. J. W. Goodman, *Speckle Phenomena in Optics: Theory and Applications* (Roberts and Company, 2007).
12. M. Mounaix, D. Andreoli, H. Defienne, G. Volpe, O. Katz, S. Grésillon, and S. Gigan, "Spatiotemporal coherent control of light through a multiple scattering medium with the multispectral transmission matrix," Phys. Rev. Lett. **116**, 253901 (2016).
13. M. Mounaix, H. Defienne, and S. Gigan, "Deterministic light focusing in space and time through multiple scattering media with a time-resolved transmission matrix approach," Phys. Rev. A **94**, 041802 (2016).
14. M. Plöschner, B. Straka, K. Dholakia, and T. Čižmár, "GPU accelerated toolbox for real-time beam-shaping in multimode fibres," Opt. Express **22**, 2933–2947 (2014).
15. N. Hagen and M. W. Kudenov, "Review of snapshot spectral imaging technologies," Opt. Eng. **52**, 090901 (2013).
16. R. Shogenji, Y. Kitamura, K. Yamada, S. Miyatake, and J. Tanida, "Multispectral imaging using compact compound optics," Opt. Express **12**, 1643–1655 (2004).
17. L. Gao, N. Bedard, N. Hagen, R. T. Kester, and T. S. Tkaczyk, "Depth-resolved image mapping spectrometer (IMS) with structured illumination," Opt. Express **19**, 17439–17452 (2011).
18. R. Content, S. Morris, and M. Dubbeldam, "Microslices and low cost spectrographs for million element integral field spectroscopy," Proc. SPIE **4842**, 174–182 (2003).
19. S. K. Sahoo, D. Tang, and C. Dang, "Single-shot multispectral imaging with a monochromatic camera," Optica **4**, 1209–1213 (2017).
20. G. Courtès, "An integral field spectrograph (IFS) for large telescopes," in *Instrumentation for Astronomy with Large Optical Telescopes*, C. Humphries, ed. (D. Reidel, 1982), pp. 123–128.
21. A. Bodkin, A. Sheinis, A. Norton, J. Daly, S. Beaven, and J. Weinheimer, "Snapshot hyperspectral imaging: the hyperpixel array camera," in *Algorithms and Technologies for Multispectral, Hyperspectral, and Ultraspectral Imagery XV*, S. S. Shen and P. E. Lewis, eds. (2009), paper 73340H.
22. M. S. Patterson, B. Chance, and B. C. Wilson, "Time resolved reflectance and transmittance for the noninvasive measurement of tissue optical properties," Appl. Opt. **28**, 2331–2336 (1989).
23. F. Van Beijnum, E. G. Van Putten, A. Lagendijk, and A. P. Mosk, "Frequency bandwidth of light focused through turbid media," Opt. Lett. **36**, 373–375 (2011).
24. B. Shapiro, "Large intensity fluctuations for wave propagation in random media," Phys. Rev. Lett. **57**, 2168–2171 (1986).
25. I. M. Vellekoop and A. Mosk, "Focusing coherent light through opaque strongly scattering media," Opt. Lett. **32**, 2309–2311 (2007).
26. N. Curry, P. Bondareff, M. Leclercq, N. F. Van Hulst, R. Sapienza, S. Gigan, and S. Grésillon, "Direct determination of diffusion properties of random media from speckle contrast," Opt. Lett. **36**, 3332–3334 (2011).
27. I. M. Vellekoop and A. Mosk, "Phase control algorithms for focusing light through turbid media," Opt. Commun. **281**, 3071–3080 (2008).
28. H. Ylmaz, W. L. Vos, and A. P. Mosk, "Optimal control of light propagation through multiple-scattering media in the presence of noise," Biomed. Opt. Express **4**, 1759–1768 (2013).
29. A. Monmayrant, S. Weber, and B. Chatel, "A newcomer's guide to ultrashort pulse shaping and characterization," J. Phys. B **43**, 103001 (2010).
30. J. Bertolotti, E. G. van Putten, C. Blum, A. Lagendijk, W. L. Vos, and A. P. Mosk, "Non-invasive imaging through opaque scattering layers," Nature **491**, 232–234 (2012).
31. S. Turtaev, I. T. Leite, T. Altwegg-Boussac, J. M. P. Pakan, N. L. Rochefort, and T. Čižmár, "High-fidelity multimode fibre-based endoscopy for deep brain in vivo imaging," Light Sci. Appl. **7**, 92 (2018).
32. A. M. Caravaca-Aguirre and R. Piestun, "Single multimode fiber endoscope," Opt. Express **25**, 1656–1665 (2017).
33. I. Gusachenko, J. Nylk, J. A. Tello, and K. Dholakia, "Multimode fibre based imaging for optically cleared samples," Biomed. Opt. Express **8**, 5179–5190 (2017).
34. E. E. Morales-Delgado, D. Psaltis, and C. Moser, "Two-photon imaging through a multimode fiber," Opt. Express **23**, 32158–32170 (2015).
35. I. Gusachenko, M. Chen, and K. Dholakia, "Raman imaging through a single multimode fibre," Opt. Express **25**, 13782–13798 (2017).
36. R. Y. Gu, R. N. Mahalati, and J. M. Kahn, "Design of flexible multi-mode fiber endoscope," Opt. Express **23**, 26905–26918 (2015).